Wind and Structures, *Vol. 19, No. 5 (2014) 541-563*
DOI: http://dx.doi.org/10.12989/was.2014.19.5.541

Field measurements of wind characteristics over hilly terrain within surface layer

Y.C. He[1], P.W. Chan[2] and Q.S. Li[*1]

[1]*Deparment of Architecture and Civil Engineering, City University of Hong Kong, Hong Kong*
[2]*Hong Kong Observatory, Kowloon, Hong Kong*

(Received January 3, 2014, Revised June 7, 2014, Accepted August 31, 2014)

Abstract. This paper investigates the topographic effects on wind characteristics over hilly terrain, based on wind data recorded at a number of meteorological stations in or near complex terrain. The multiply data sources allow a more detailed investigation of the flow field than is normally possible. Vertical profiles of mean and turbulent wind components from a Sodar profiler were presented and then modeled as functions of height and wind speed. The correlations between longitudinal and vertical wind components were discussed. The phenomena of flow separation and generation of vortices were observed. The distance-dependence of the topographic effects on gust factors was revealed subsequently. Furthermore, the canyon effect was identified and discussed based on the observations of wind at a saddle point between two mountain peaks. This study aims to further understanding of the characteristics of surface wind over rugged terrain. The presented results are expected to be useful for structural design, prevention of pollutant dispersion, and validation of CFD (computational fluid dynamics) models or techniques over complex terrains.

Keywords: wind characteristics; hilly terrain; profile; flow separation; canyon effect; topographic effect

1. Introduction

Hilly terrain may result in complex flow phenomena such as development, separation, reattachment and downstream recovery of the turbulent boundary layer. Thus, wind characteristics over hills usually demonstrate markedly different features from those under open flat terrain conditions. A well-known feature is the speed-up effect near hill crest that has been stipulated in the wind load codes of several countries (AIJ 2004, GB50009-2012 2012). In case of sufficiently steep hills, flow separations may occur (Wood 1995), which may affect the wind structure remarkably. It was reported that the geometry and vegetation coverage (or roughness) of hills also affect the structure of both mean and fluctuating wind components (Lemelin *et al.* 1988, Cao and Tamura 2006, Cao *et al.* 2012).

During the last decades, quite a number of researches have been focused on this subject to cater for the estimations of wind energy, wind loads for structural designs, dispersion of pollutants and so on under complex hilly terrains (Mengelkamp 1998, Baker *et al.* 1985, Apsley and Castro 1997). According to Wood (2000), studies on the wind characteristics under hilly terrains started from the

*Corresponding author, Professor, E-mail: bcqsli@cityu.edu.hk

http://www.techno-press.org/?journal=was&subpage=8 ISSN: 1226-6116 (Print), 1598-6225 (Online)

1930s based on simple phenomenological observations. Theoretical analysis of non-viscous flows over hills came out in the 1950s, which was developed into a more mature research topic of viscous flow since the 1970s.As the fast development of CFD techniques and wind tunnel tests in recent years, more related studies have been conducted by numerical and wind tunnel investigations.

Among those studies, as a pioneering work, Jackson and Hunt (1975) developed a linear 2D theory (JH theory) for flow perturbations induced by hills with low height-length aspect ratio. This theory predicts that a hill affects the flow past it by inducing a negative pressure perturbation at the hill crest and a positive pressure perturbation downstream the hill. As a result, flow on the upstream slope is accelerated, while that over the downstream slope is decelerated. They divided the atmosphere around the hill into two layers: the outer layer and the inner layer. The outer layer is assumed to be essentially inviscid and driven by external pressure, while the inner layer is dominated by the turbulent stresses. In particular, the inner layer depth can be simply regarded as the height where the maximum speed-up appears (Taylor *et al.* 1987).

The JH theory was further expanded from 2D to 3D by Mason and Sykes (1979). These two studies triggered more following investigations and achievements (Taylor 1998), such as the development of MS3DJH model (Walmsley *et al.* 1982), the MSFD model (Beljaars *et al.*1987), the NLMSFD model (Xu *et al.* 1994), and the HRB model (Hunt *et al.* 1984) and HLP model (Hunt *et al.* 1988).Some results of the previous studies have been adopted in the wind codes of several countries (ASCE7 2005, GB50009 2012,Ngo and Letchford 2008).

The JH theory considered the case with no mean flow separations. But under certain conditions, air flow may separate at hill sides (Wood 1995, Griffiths and Middleton 2000). When separation occurs, the formed vorticities can be transported far away from the surface into both the inner and outer layers. Consequently, the flow structures would be changed remarkably, and the perturbation component of wind speed becomes comparable to the mean flow component. Such features make it very difficult to accurately predict the turbulent wind characteristics at the leeward side of hills via numerical simulations (Derickson and Peterka 2004, Cochran and Derickson 2011). For 2D hills, the separation phenomenon is usually featured by reversed flows. For 3D hills, however, recirculating flows with closed streamlines may be hardly observed (Hunt *et al.* 1978). In this case, separation can be regarded to occur if the detected mean wind speed is reduced evidently (less than half the speed of upstream wind) and the turbulence increases significantly (larger than twice the turbulence of upstream wind) (Taylor *et al.* 1987). A field study on wind flow over a 3D hill by Mason and King (1985) showed that separation would occur when the fractional steep slope is larger than 0.35. But, the observations from a 2D hill with the slope larger than 0.45 revealed no typical reversed flows (Taylor *et al.* 1987). Apart from these field measurement studies, Wood (1995) deduced an estimator of the critical slope for the onset of separation through theoretical analysis.

Great efforts have been made to explore the complexity of turbulent wind characteristics under rugged terrain conditions via wind tunnel tests, numerical simulations and other methods (e.g., Takahashi 2002, Keith 2004, Cao *et al.* 2006, Tamura *et al.* 2007a, b). Among these studies, field measurements have played an important role in the development of the research works on this topic(Taylor *et al.*1987), as they provided the primary source for further theoretical and numerical analyses, and also served as the most credible tool to verify the validity of the proposed theories and models. A comprehensive collaborative study of the Askerve in Hill Project was carried out during the 1980s (Taylor and Teunissen 1987, Walmsley and Taylor 1996). The vertical profiles of wind and turbulence (Mickle *et al.* 1988) and mean wind variations at fixed heights above ground

(Salmon *et al.* 1988) were presented and discussed. Other field studies included the measurements of mean flows over the Cooper's Ridge under both near-neutral and non-neutral thermal conditions (Coppin *et al.* 1994), the estimation of topographical exposure factors under hilly terrain conditions (Baker 1984), the determination of wind profile constants under neutral conditions over complex hilly terrain (Kustas and Brutsaert 1986), and the measurement and interpretation of peak-gust wind speeds over an isolated hill (Bowen and Clucas 1992). Although a number of field measurement studies have been conducted, detailed observations of wind structures based on multiply data sources over complex hilly terrains have rarely been reported.

Hong Kong is sited on the southeast coastal line of China and may be attacked by strong wind storms such as tropical cyclones every year. The regional topography is quite complicated and dominated by irregular hills and mountains. As an international metropolis, Hong Kong is featured by high density of population and large-scale civil structures. The potential danger for populations, aircrafts and civil structures against severe winds, outdoor fires, and air pollutions makes it of great importance to clarify the topographic effects on the wind characteristics over complex terrains. This paper presents an investigation of wind profiles and turbulence characteristics of surface wind based on the wind data recorded from a Sodar profiler system and anemometers during long-term field measurements at several meteorological stations around Hong Kong International Airport (HKIA).

The contents of this paper are arranged as follows: the information of the meteorological stations and wind data sets used in this study will be introduced in Section 2. Results from a Sodar profiler system will be presented and discussed in Section 3. In the next three sections, flow separations, characteristics of gust factors, and canyon effect will be studied. Main findings and conclusions will be summarized in Section 7.

2. Meteorological stations and data quality control

2.1 Locations of the meteorologicalstations

An overall view of the study area and its surrounding regions is shown in Fig. 1(a). Fig. 1(b) shows the distribution of the meteorological stations around HKIA which is sited at the northwest of the Lantau Island. There are three transects which are respectively denoted as Ti, i=1,2,3, with each transect crossing through several stations. The stations in Ti are respectively denoted as $T_i^j, j = 1,2,3, \ldots$ along the direction toward the arrowed side. Other stations without names marked in Fig. 1(b) will not be considered in the following analysis. Among the stations, those marked with blue circles are buoy sites; the ones with red squares are general meteorological stations; while those with black triangles are the stations built on mountains. All these stations are equipped with mechanical anemometers (buoy sites with propeller type anemometers, others with cup type anemometers)for detection of horizontal component of wind at the fixed heights as listed in Table 1. In particular, Sui Ho Wan (SHW) meteorological station marked with red star in Fig. 1(b) is equipped with both an anemometer and a Doppler Sodar profiler system. It is located at the northeastern part of Lantau Island and is in front of the runway of HKIA. The CCH and WGL stations are also included in the figures, which serve as the reference stations for comparison purposes only.

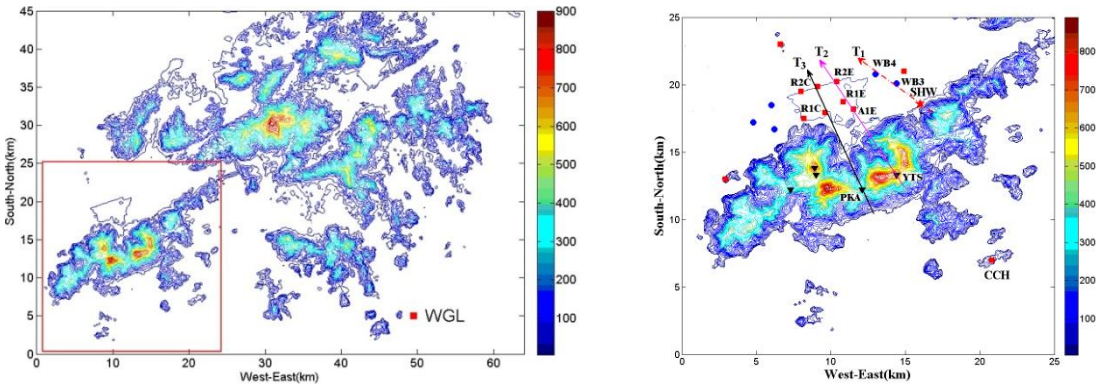

(a) Over view (b) Zoomed view

Fig. 1 Locations of selected meteorological stations (white color stands for the mean sea level, (b) corresponds to the region delineated by the red rectangle in (a))

Table 1 Elevations of local ground (G) above mean sea level and anemometer (A) above mean sea level/local ground of the stations

$\rightarrow$	T_i^1		T_i^2		T_i^3		T_i^4	
	Site	Height(m)	Site	Height(m)	Site	Height(m)	Site	Height(m)
T_1	SHW	G: 5 A: 15/10	WB3	G: 0 A: 8.5/8.5	WB4	G: 0 A: 8.5/8.5	--	--
T_2	YTS	G: 742 A: 752/10	A1E	G: 5 A: 15/10	R1E	G: 5 A: 15/10	R2E	G: 5.2 A: 15.2/10
T_3	PKA	G: 371 A: 386/15	R1C	G: 3.2 A: 13.2/10	R2C	G: 3.7 A: 13.7/10	--	--
Reference stations	CCH	G: 71.9 A:98.6/26.7	WGL	G: 55.8 A:82.7/26.9				

2.2 Dataset and data quality control

All the stations marked in Fig. 1(b) can provide minute-to-minute updated wind records which consist of 1min non-overlapping scalar mean wind speed and direction and 3sec peak gust, based on the instantaneous readings sampled at 1 Hz. Six years' database collected from these stations during 2005-2010 is adopted for analysis in this study. Meanwhile, another 45 days' records updated every second are also available, which were collected during a number of strong wind events at SHW.

In statistical analysis, control tests for examining the data quality should be conducted. For the anemometers' records, this study follows the way introduced in Masters *et al.* (2010) which mainly considered tests for thermally neutral stability and for stationary. Specifically, (1) the mean wind speed should not be less than 5 m/s; (2) the difference between the scalar and vector mean wind speeds should be less than 0.6 m/s; (3) the standard deviation of wind direction should be less than

20°; (4) peak gust speed should be constrained within 6 times the standard deviation of speed away from the mean; (5) each segment of wind speed time series should pass through the 1storder stationary test at a significance level of 0.05, by using the reverse arrangement approach.

The Doppler Sodar profiler system at the SHW station (Aero Vironment model 4000) operates at an acoustic frequency of 4.5 kHz. It probes the three components of wind velocity up to a height of 100 m above ground level using a vertical beam and two oblique beams at 15 degrees from the vertical (Chan 2008). The records from the system, which were updated every 5 minutes, covered a detecting range from 5 m to 100 m above ground with 5 m interval. But, due to nearby obstructions, the records at the lowest gate levels of 5-20 m were influenced evidently by surroundings. Thus, these records will be discarded in the following analysis. The recorded segmental information at each gate level includes: the spatial velocity vectors of mean and turbulent (in terms of standard deviation) wind components along 3 orthogonally distributed directions and the SNR (signal to noise ratio) index values of the corresponding beam signals. In this study, the gate records with SNR values of all the 3 velocity components no smaller than 8 are regarded as credible. A profile with at least 13 credible gate records (totally 16) is regarded acceptable. All the analysis presented below is based on the acceptable profiles selected from a 3 years' dataset recorded during 2008-2010.

It is noteworthy that the Sodar profiler system may lose efficiency in case of heavy rain. Data collected from the system under such a condition are probably rejected through the above quality control process. But, as strong winds are usually accompanied with heavy rains, a considerable amount of the measurements recorded during high wind speeds may be excluded. Another point to be noted is that the Sodar system can only detect components of wind vector along the vertical direction (w), and two orthogonally distributed horizontal directions (x, y). The longitudinal mean wind speed U, the effective standard deviation σ_u, and the effective turbulence intensity I_i (the effective value is adopted to distinguish it from the traditional form) are calculated by the following expressions

$$\mathrm{U} = \sqrt{U_x^2 + U_y^2},\ \sigma_u = \sqrt{\sigma_x^2 + \sigma_y^2}, I_i = \frac{\sigma_i}{U}, i = u, w \tag{1}$$

where, $\sigma_x, \sigma_v, \sigma_w$ are the standard deviation of wind components along direction x, y and w.

3. Results from the Sodar profiler at SHW station

3.1 Reference speed and direction

First of all, the records from the Doppler Sodar system are analyzed. The analysis is conducted in a composite sense, following the way adopted in Powell *et al.* (2003), and Tamura *et al.* (2007). The qualified datasets are stratified according to the reference wind speed $\mathrm{U_{ref}}$ and direction θ_{ref} which is respectively defined as the arithmetic average speed and the vector average direction of the horizontal wind components at all the considered gates within 25-100 m. Wind direction is defined as positive clockwise from the north (or 0°).Similarly, the vertical reference wind speed $\mathrm{W_{ref}}$ is defined as the scalar average of the vertical wind speeds within 25-100 m.

To balance the category of upwind terrains and the amount of selected datasets, the full azimuth at the SHW station is uniformly divided into 6 sections clockwise from the north, which are denoted as θi (i=1, 2, 3, 4, 5, 6). This study only considers two typical sections: θ2 (60-120°) and

θ6 (300-360°) which correspond to the upwind and downwind hilly exposure conditions, respectively. The reference wind speeds U_{ref}, or the scalar average of all gate speeds, are divided into groups with an incremental step of 3m/s (the first group: 0-3 m/s), which are denoted as Vi (i=1, 2, 3…).

3.2 Vertical profiles

Fig. 2 shows the vertical profiles of the normalized longitudinal mean wind speed by the reference speed U_{Norm}, the vertical mean wind speed W, and the horizontal effective turbulence intensity I, based on the profiles whose reference speeds are not less than 5 m/s. The bilateral error-bars represent ±1 standard deviation from the mean value. Numbers of individual profiles N are also presented. Each ensemble-mean profile is fitted by the power-law (green line), the log-law (red dash line), and the linear-log law (magenta line) which will be discussed in details later.

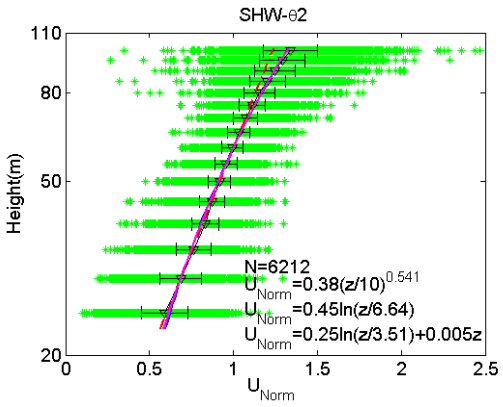

(a) Normalized longitudinal speed in θ2

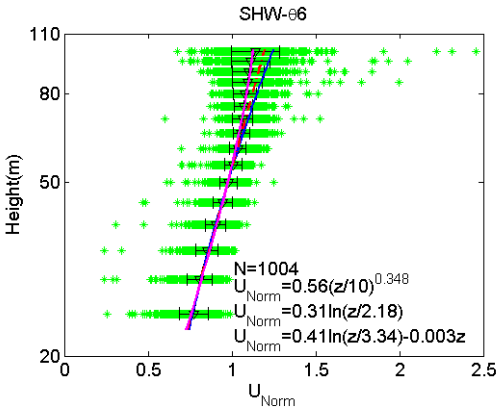

(b) Normalized longitudinal speed in θ6

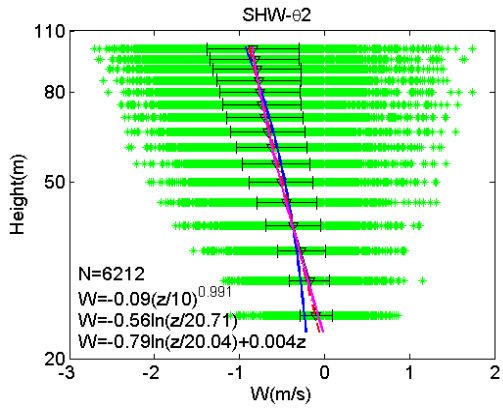

(c) Vertical speed in θ2

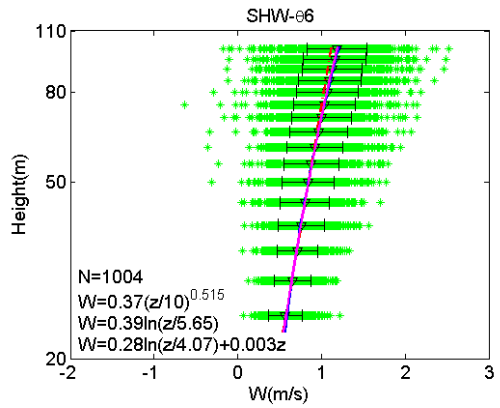

(d) Vertical speed in θ2

Continued-

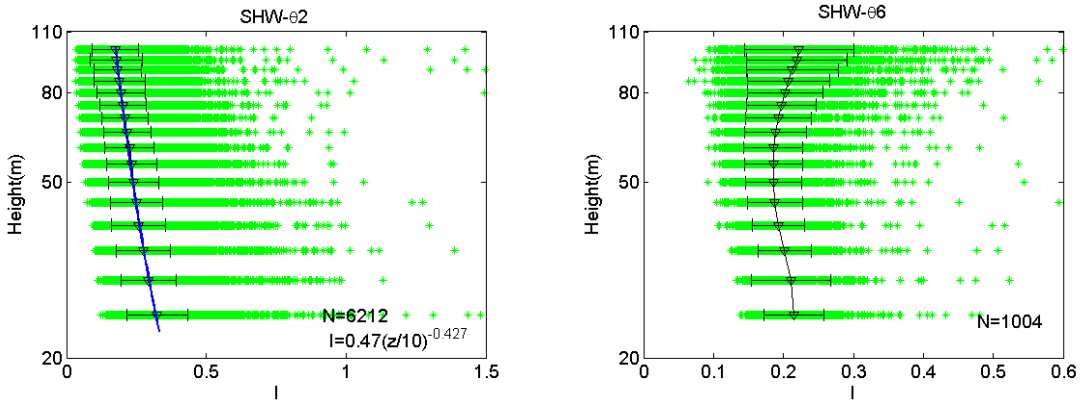

(e) Effective turbulence intensity in θ2 (f) Effective turbulence intensity in θ6

Fig. 2 Mean wind profiles of normalized longitudinal speed, vertical speedand effective horizontal turbulence intensity. Triangles stand for the ensemble mean values. The bilateral error-bars represent ±1 standard deviation from the mean.Each ensemble-mean profile is fitted by the power-law (green line), the log-law (red dash line), and the log-linear law(magenta line)

As can be seen, the wind profiles in both azimuthal sections demonstrate some markedly different features from those over open terrains (under neutral condition): (1) the ensemble-mean speeds do not increase logarithmically with altitudes at upper heights: those in section θ2 are accelerated more rapidly while the ones in section θ6 tend to level off; (2) the vertical speed is not zero, evident downward and upward wind flows were observed in sections θ2 and θ6, respectively, with the absolute values increasing logarithmically with height.

Figs. 3 and 4 depict the ensemble-mean profiles by groups of the reference speeds in sections θ2 and θ6. The following features can be observed based on these results: (1) the longitudinal and vertical wind components are closely correlated with each other. Stronger horizontal winds correspond to larger $|W|$ values; (2) the mean speed profiles in both sections deviate from the log-law predictions. The heights where the measurements become to depart from the log-law predictions decrease with wind strength; (3) the distributions of the profiles of $\sigma_i, I_i, i = u, v$are quite complicated. Results in the same section demonstrate similar tendency, but those in different sections vary remarkably.

The log-linear law, deduced from the Monin-Obukhov similarity theory (Garratt 1992), is adopted to quantify the obtained ensemble-mean profiles

$$\mathrm{U(z)} = \left(\frac{u_{*0}}{\kappa}\right)\ln\left(\frac{\mathrm{z}}{z_0}\right) + \xi\mathrm{z} \tag{2}$$

where κ=0.4 is the von Karman constant;$u_{*0}$is the surface friction velocity;z_0 is the roughness length scale;ξ is the stability parameter,with ξ>0 and ξ<0 corresponding to downward convection and upward convection, respectively. The height coordinate z stands for the elevation above local ground, i.e., the zero-displacement planed is considered as zero. Under rough terrain conditions, d should usually be taken into account in modelling a profile. In general, this parameter may lead to the best fitting of a profile (Stearns 1970, Wiggs *et al.* 1996). However, this parameter is not considered herein, since it was found that there was nearly no improvement of the fitting results by introducing the item.

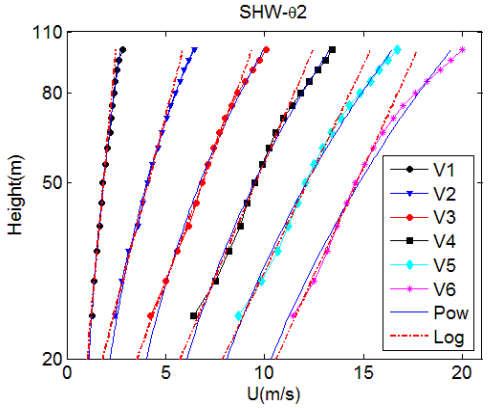

(a) Longitudinal speed

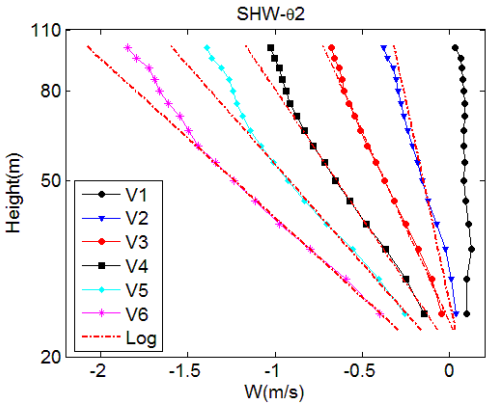

(b) Vertical speed

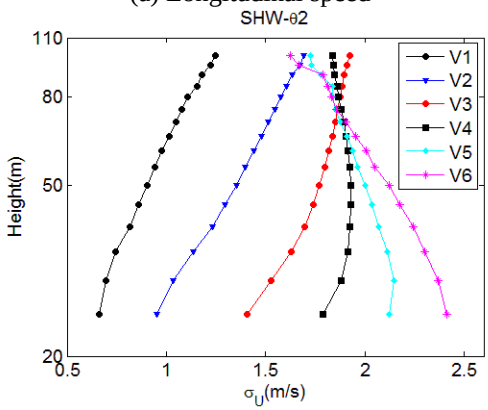

(c) Variance of longitudinal speed

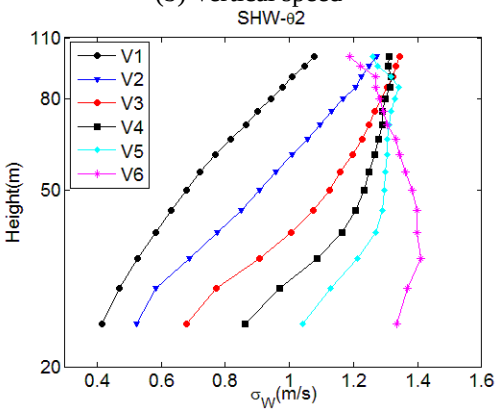

(d) Variance of vertical speed

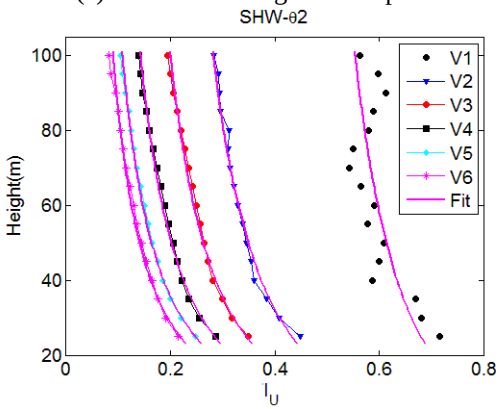

(e) Turbulence intensity of longitudinal speed

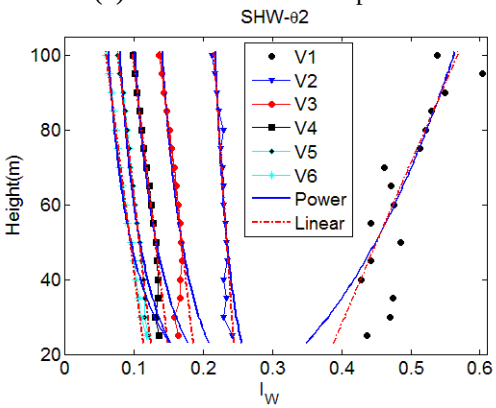

(f) Turbulence intensity of vertical speed

Fig. 3 Ensemble-mean profiles insection θ2

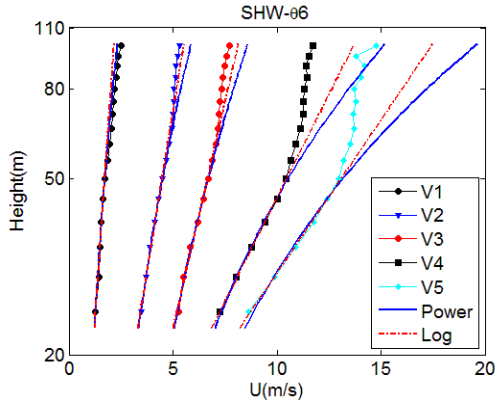

(a) Longitudinal speed

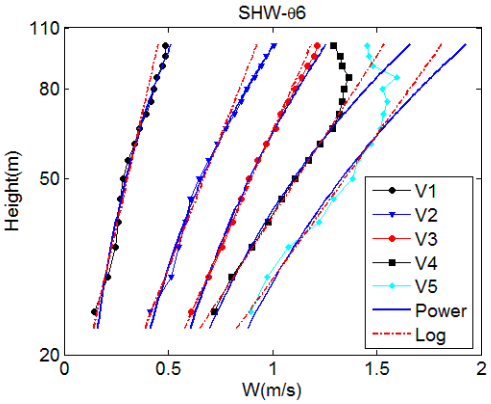

(b) Vertical speed

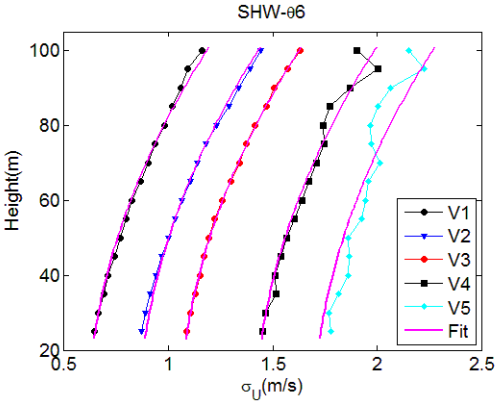

(c) Variance of longitudinal speed

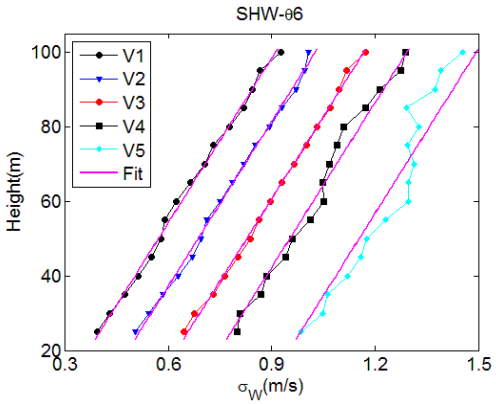

(d) Variance of vertical speed

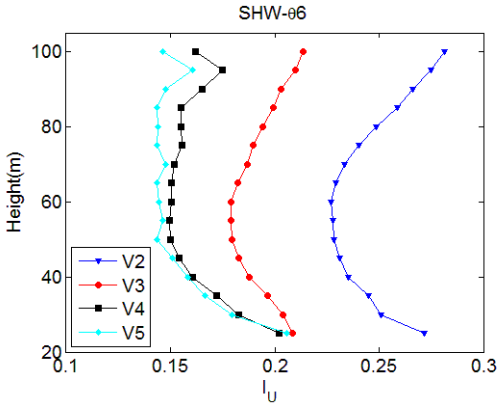

(e) Turbulence intensity of longitudinal speed

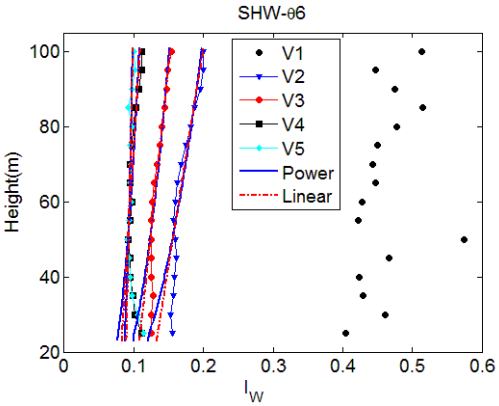

(f) Turbulence intensity of vertical speed

Fig. 4 Ensemble-mean profiles in section θ6

The fitting results are shown in Fig. 5 and Tables 2-3. In Fig. 5, ensemble-mean profiles in the V4 speed group are extracted to provide a comparison of the regression results by using the following models: power law (Power), log-law (Log-1), and log-linear law (Log-linear). Meanwhile, the results based on the truncated log-law (Log-2) from the log-linear fitting results by setting $\xi = 0$ while other parameters kept unchanged are also depicted to highlight the role of the ξ item (corresponding to the difference between Log-linear and Log-2, as marked by the green arrow lines) in the profiles. In Tables 2 and 3, "N" is the amount of profile samples, $U_{ref}, W_{ref}, \sigma_{ref}$ represent the ensemble-mean reference values, defined as the scalar average of all height levels of the ensemble-mean profile, of the corresponding quantities.

Table 2 Fitting results of longitudinal wind profiles (N: specimen number; R^2: fitting goodness)

					Power Law			Log Law		Log-linear Law			
	Vi	*N*	U_{ref}	σ_{ref}	U_{10}	α	R^2	u_*	z_0	u_*	z_0	ξ	R^2
	*V*2	2752	4.61	1.41	1.39	.665	.997	1.02	9.9	.592	7.4	.025	.998
	*V*3	2573	7.50	1.78	2.72	.564	.993	1.44	7.5	.864	4.7	.033	.994
θ2	*V*4	1944	10.4	1.88	4.32	.488	.993	1.67	5.1	.892	2.0	.046	.994
	*V*5	633	13.1	1.93	5.96	.442	.993	1.86	3.7	.868	.77	.060	.995
	*V*6	90	15.9	2.01	7.84	.394	.984	1.78	1.9	.808	.22	.072	.991
	*V*1	396	1.93	.867	.80	.495	--	.324	5.5	.166	1.9	.0084	.994
	*V*2	1164	4.65	1.11	2.47	.369	--	.628	2.8	.844	4.3	-.014	.993
θ6	*V*3	491	6.82	1.31	3.92	.325	--	.820	2.0	1.16	3.5	-.021	.992
	*V*4	46	10.4	1.67	5.24	.409	--	1.592	3.9	2.89	7.1	-.076	.996
	*V*5	10	12.8	1.95	6.41	.414	--	2.00	4.1	3.78	7.5	-.103	.982

Table 3Fitting results of vertical wind profiles

					Power Law		Log Law			Log-linear Law			
	Vi	*N*	W_{ref}	σ_{ref}	W_{10}	α	u_*	z_0	R^2	u_*	z_0	ξ	R^2
	*V*2	2752	-.198	.981	--	--	-.095	27	.915	-.048	48	-.0029	.977
	*V*3	2573	-.436	1.14	--	--	-.201	24	.996	-.234	22	.0019	.997
θ2	*V*4	1944	-.718	1.22	--	--	-.297	21	.998	-.404	19	.0065	.998
	*V*5	633	-.992	1.27	--	--	-.387	19	.996	-.528	18	.0093	.997
	*V*6	90	-1.33	1.32	--	--	-.484	18	.995	-.636	17	.0103	.998
	*V*1	396	.374	.655	.084	.785	.084	184	--	.042	9.5	.0026	.988
	*V*2	1164	.751	.771	.251	.601	.146	7.9	--	.064	3.3	.0048	.996
θ6	*V*3	491	.975	.912	.401	.494	.165	5.6	--	.131	4.4	.0020	.999
	*V*4	46	1.02	1.04	.430	.584	.238	7.7	--	.416	10	-.010	.978
	*V*5	10	1.38	1.24	.567	.530	.266	6.6	--	.444	10	-.018	.968

As can be seen, fittings of the log-linear model show desirable agreement with the measurements, with the least fitting goodness value R^2 no less than 0.96. As expected, the parameter ξ for U is positive in section θ2 and negative in sectionθ6 under stronger wind conditions. It seems that ξ serves as a measure of the terrain relief (rising or falling), compared to its original meaning of the stability state of the atmosphere. It is also observed that the absolute values of ξ increase consistently with U_{ref} in both azimuthal sections, implying that the to pographic effects on the surrounding wind field tend to be more significant under stronger wind conditions.

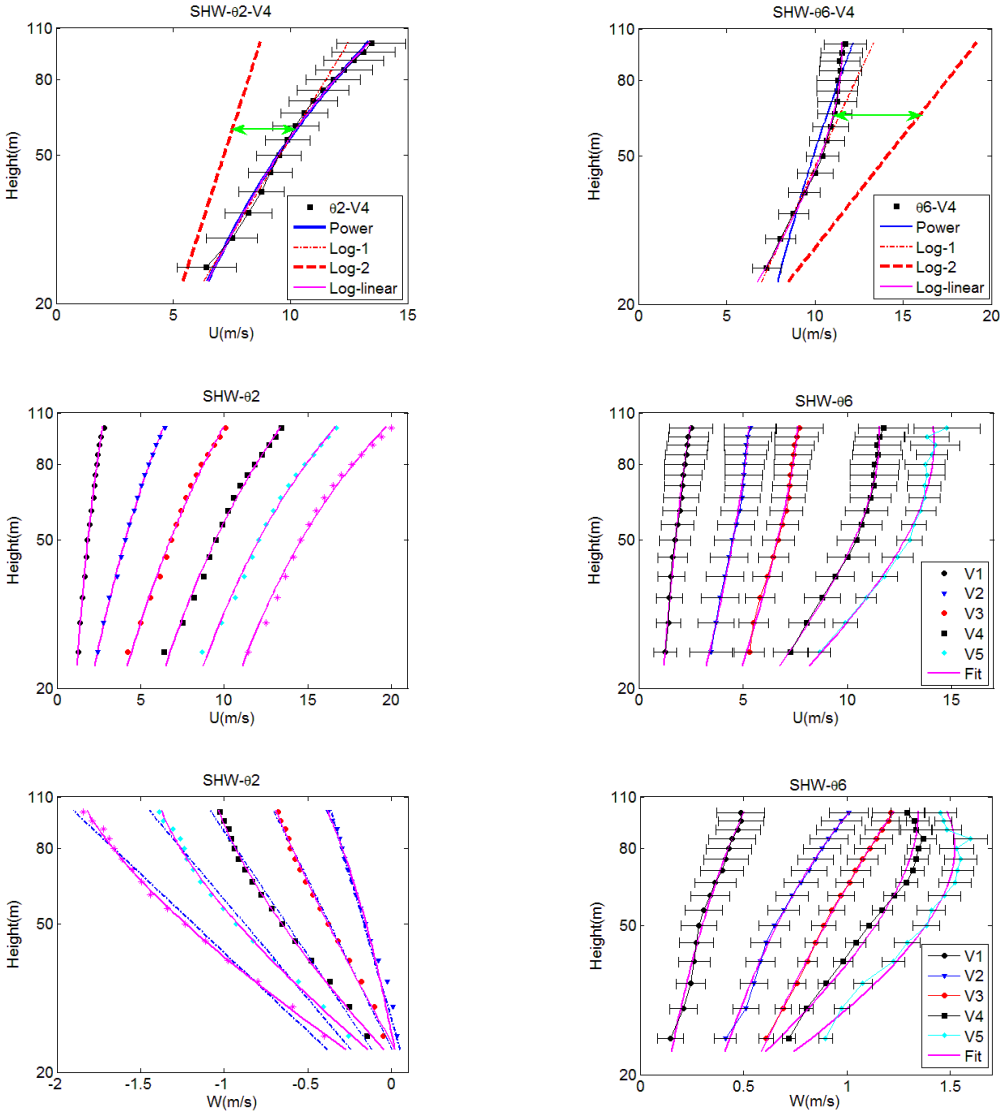

Fig. 5 Ensemble-mean profiles fitted by the log-linear law

3.3 2D Empirical wind profile models

From the above analysis, all the profiles are dependent upon both height and wind strength. This section aims to establish 2D empirical models of the obtained profiles as functions of these two parameters.

3.3.1 Correlations between horizontal and vertical speeds

The correlations between the horizontal and vertical mean wind components can be formulated by the following equations

$$U_{ref,\theta 2} = \sqrt{30.3 - 320W_{ref} - 5.50} \tag{3}$$

$$U_{ref,\theta 6} = 4.84W_{ref}^2 + 2.87W_{ref} \tag{4}$$

where, the items on the left sides of the above equations have a unit of m/s, and θ2 and θ6 in the subscripts stand for the azimuth sections, hereafters.

3.3.2 Profiles of horizontal wind speed

The three parameters involved in the log-linear law (Eq. (2)) for the horizontal wind speeds are modelled by the following fitting equations

$$u_{*,\theta 2} = -0.0072U_{ref}^2 + 0.162U_{ref}, u_{*,\theta 6} = 0.058U_{ref}^{1.646} \tag{5}$$

$$z_{0,\theta 2} = e^{-0.312U_{ref}+3.71}, \quad z_{0,\theta 6} = e^{0.119U_{ref}+0.599} \tag{6}$$

$$\xi_{\theta 2} = 4.54 \times 10^{-3}U_{ref}, \xi_{\theta 6} = -6.39 \times 10^{-4}U_{ref}^2 \tag{7}$$

Substituting the above equations into Eq. (2), the longitudinal mean wind profiles within the surface layer can be predicted.

3.3.3 Profiles of turbulence

The standard deviation of wind speed σ and the effective turbulence intensity I can be calculated from each other through Eq. (1). From Figs. 3 and 4, it is advisable to modelI first and then to model σ for section θ2. For section θ6, the procedure is opposite, i.e., it's more appropriate to determine σ first and thenI. The obtained modeling results are given as follows

$$I_{u,\theta 2} = (0.047U_{ref} + 0.947)z^{(-0.035U_{ref}-0.118)} \tag{8}$$

$$I_{w,\theta 2} = \left(1.97 \times \frac{10^{-3}}{U_{ref}} - 8.24 \times 10^{-4}\right)z + 0.568U_{ref}^{-0.533} \tag{9}$$

$$\sigma_{u,\theta 6} = (5.7 \times 10^{-5}z^2 + (0.099U_{ref} + 0.402) \tag{10}$$

$$\sigma_{w,\theta 6} = 6.8 \times 10^{-3}z + (0.052U_{ref} + 0.118) \tag{11}$$

3.3.4 Correlation of standard deviations

The effective standard deviations of the horizontal and vertical wind components are positively correlated. Fig. 6 shows the profiles of σ_w/σ_u in both sections θ2 and θ6. For neutral stratified

atmosphere over open flat terrain, the relationship between σ_u and σ_w can be depicted by the following equation which is recommended in ESDU-85020 (1985)

$$\sigma_w/\sigma_u = 1 - 0.45cos^4(\frac{\pi z}{2h_B}) \tag{12}$$

where, $h_B = u_*/(6f_c)$is the depth of the atmospheric boundary layer with a typical value ranging from 1000 m to 3000 m, f_c is the Coriolis parameter. Predictions from this equation with $h_B = 1000$ m (denoted as ESDU-1) and $h_B = 3000$ m (ESDU-2) also shown in Fig. 6. As can be seen, the results are insensitive to h_B within the surface layer, and the value of σ_w/σ_u is almost kept constant along height. However, the measurement results show remarkable deviation from the ESDU predictions, reflecting the fact that turbulent characteristics of wind flows around hills are closely related to local topographic features. To model the profiles of σ_w/σ_u, the following formula is considered

$$\sigma_w/\sigma_u = 1 - a\ln^b(L/z) \tag{13}$$

where, a, b are two coefficients to be determined, with a serving as alocation parameter to determine the location of σ_w/σ_u in abscissa and b serving as a shape parameter to determine the concavity of the profile; Lis the half-height length of the hill, which is defined as the horizontal distance between the hill crest and the location where the altitude to ground is half the crest height.

The fitting results are also depicted in Fig. 6. The two coefficients are a=0.116 and b=1.27 for section θ2, and a =0.094 and b=1.12 for section θ6, respectively. It is found that the coefficient a may be related to the distance between the hill crest and the study site; while the coefficientbis expectedto be dominated by the steep slope of the hill at the windward side. Asbbecomes smaller, the profile tends to level off. When it becomes sufficiently small (e.g., 0.1), by adjusting the value of a (0.4), a similar profile as predicted by Eq. (13) can be achieved.

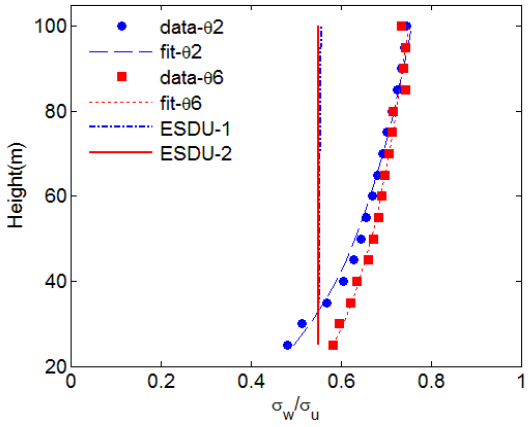

Fig. 6 Profiles of σ_w/σ_u

4. Flow separations

As discussed in the introduction section, when the steep slope θ_s (defined as $\theta_s = H/L$) of a hill becomes large enough, separation phenomenon may occur. It is found that the values of θ_s of upwind hills around SHW in section $\theta 2$ are sufficiently large (>0.45). Thus, flow separation may occur on the hill's sides. Here, the measurements during two strong wind events will be discussed. One wind event is the Severe Tropical Storm Kammuri, which resulted in the issuance of No. 8 Gale or Storm Signal by Hong Kong Observatory (HKO). The other event is a strong monsoon during 29th Sep., 2009 for which HKO issued the Strong Monsoon Signal. Detailed information of these two events can be found in the website of HKO: http://www.hko.gov.hk/cis/warndb_c.htm.

The measurements at five stations are considered herein: SHW, WB3, WB4, CCH, and WGL. As shown in Fig. 1(b), the first three stations are located in the transect T1. CCH and WGL are located atop the local islands. Thus, the records collected at these two stations are expected to be less affected by evident sheltering effects, although they may be influenced by the speed-up effect.

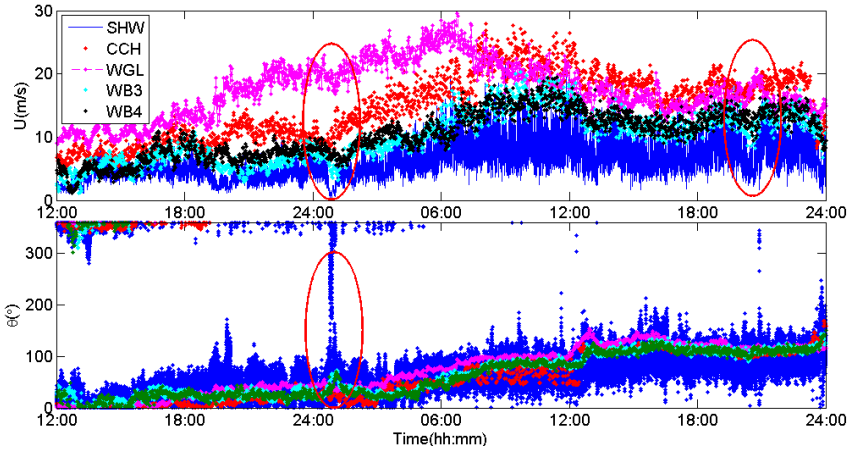

(a) 12:00 on 5th to 24:00 on 6th Aug. 2008

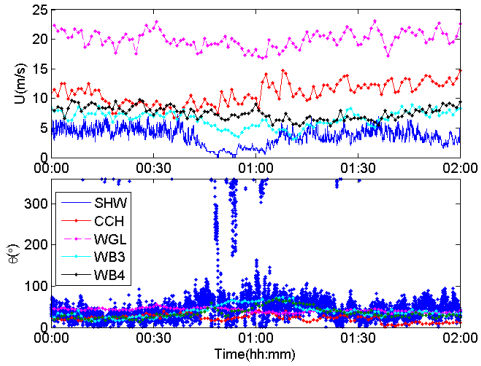

(b) 00:00-02:00 on 6th

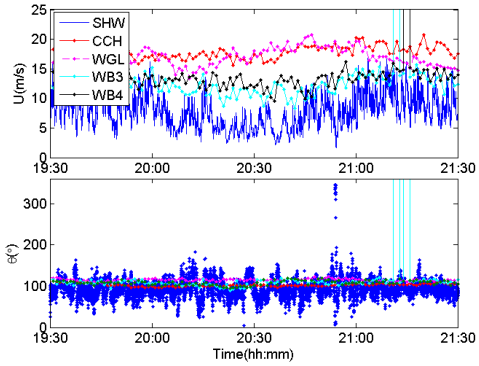

(c) 19:30-21:30 on 6th

Fig. 7 Wind speed and direction during Kammuri coming close to Hong Kong

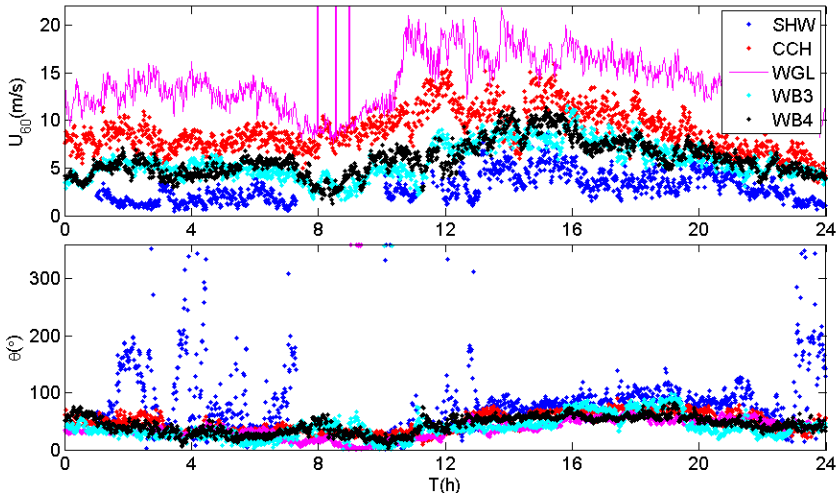

Fig. 8 Wind records during a strong monsoon event on 29th, Sep. 2009

Fig. 7 shows the time series of wind speed and direction at these stations during the period when Kammuri came close to Hong Kong from 12:00 on 5thAug., 2008 to 24:00 on 6thAug., 2008. The records at SHW were extracted from the second-to-second updated anemometer data, while the others were extracted from minute-to-minute updated data.

In Fig. 7(a), there are two marked time segments delineated by red circles: one is around 01:00, and the other is around 20:30. Within these two segments, wind speeds at SHW were remarkably reduced, compared to those at the other stations. The wind direction in the first marked segment changed severely. The records at WB3 and WB4 demonstrated a similar trend with that at SHW. The local views of these two segments are shown in Figs. 7(b) and 7(c). It is observed that the wind speed around 01:00 at SHW approached to zero. Especially, the wind direction reversed during this period (60°-70° changed to 240°-250°), although with quite short lasting durations (1 or 2 minutes). Thus, it is believed that separation occurred.

Fig. 8 shows the minute-to-minute updated 1 min mean wind speed and direction at the five stations during the strong monsoon event. It is clear that wind direction reversed around 02:00 and lasted for about an hour. The corresponding wind speeds, although quite small, were nonzero. There are also several similar segments. Therefore, it is considered that vorticities were formed and moved downwind which led to the generation of reversed flows. But, we didn't observe any such reversed flows at WB3 and WB4. Therefore, it is postulated that the formed vorticities scattered and disappeared rapidly before reaching farther to the WB3 station.

5. Turbulence characteristics of surface wind

This section focuses on the turbulence characteristics of surface wind based on the measurements recorded from the meteorological stations in transects T1 and T2 shown in Fig. 1. Gust factors with respect to different gust durations (gust factor curves) will be determined statistically, based on the qualified 1h length segments of the records. Conventionally, gust

factor $GF_{(\tau,T_0)}$ is defined as a ratio of the peak gust $\hat{u}(\tau,T_0)$over gust duration τ to the mean wind speed U over a period T_0 (unit: second)

$$GF_{(\tau,T_0)} = \hat{u}(\tau,T_0)/U(T_0) \tag{14}$$

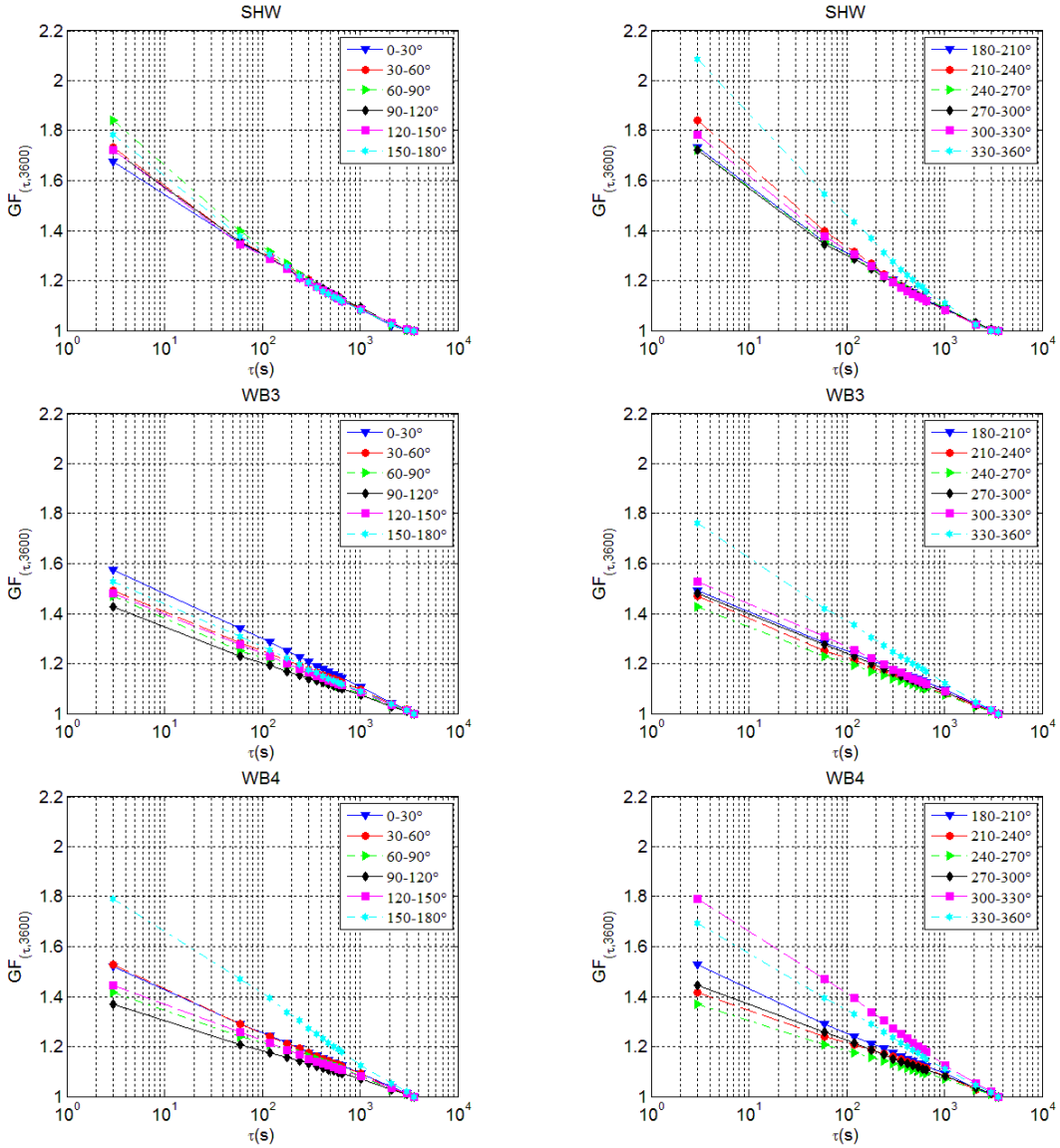

Fig. 9 Gust factor curves of the horizontal and transverse wind components

We set $T_0 = 3600, \tau = 3,30,120,180,\ldots,3600$, and follow the method presented in He *et al.* (2013) for the calculation of $GF_{(\tau,T_0)}$. The large amount of minute-to-minute updated records at these stations allows a more refined stratification of the azimuth. Hence, 12 uniformly divided sections are considered herein. The mean values of $GF_{(\tau,T_0)}$ with respect to varied gust durations in these sections at the stations in T1 and T2 are shown in Figs. 9 and 10, respectively.

Due to the complexity of the surrounding topographic features, values of $GF_{(\tau,T_0)}$ in different sections were found to vary remarkably. The obstructions of Tai Mo Shan and Lantau Island in the northern, southeastern and southern azimuths may result in flow separations and vortex shedding at their leeward sides which would then aggravate the wind shear and turbulence near the surface level (Chan 2014).

Among these stations, YTS is located atop one Peak of Lantau Island. Although the mean wind speeds were supposed to be influenced due to the speed-up effect, the much smaller values of the gust factor there indicate that the wind flows were not disturbed evidently by the mountain.

To study the distance dependency of the topographic effects on the wind turbulence, Fig. 11 compares $\mathrm{GF}_{(\tau,\mathrm{T}_0)}$ values at different sites along T1 and T2. Prediction values at 10 m height over open flat terrain with a number of roughness lengths via the ESDU (Engineering Science Data Unit) model (ESDU 1983) are also depicted. As expected, the field measurement results demonstrate an anti-correlation with the horizontal distances of station site away from the mountain-top: A1E>R1E>R2E, SHW>WB3>WB4.

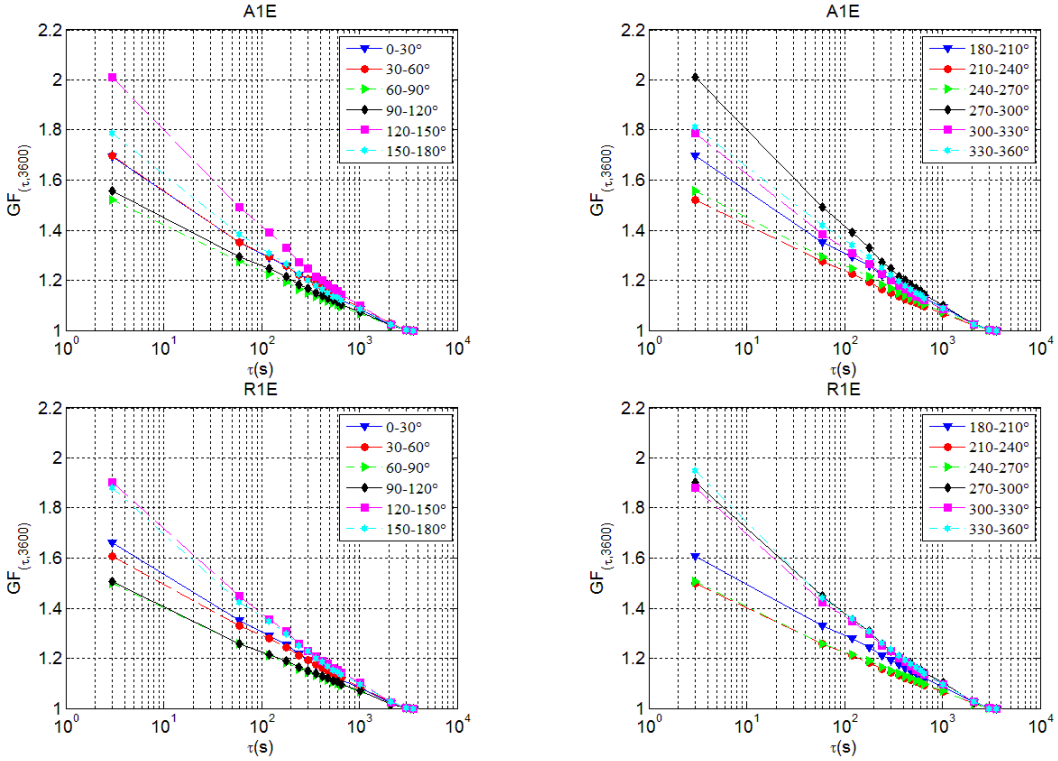

Continued-

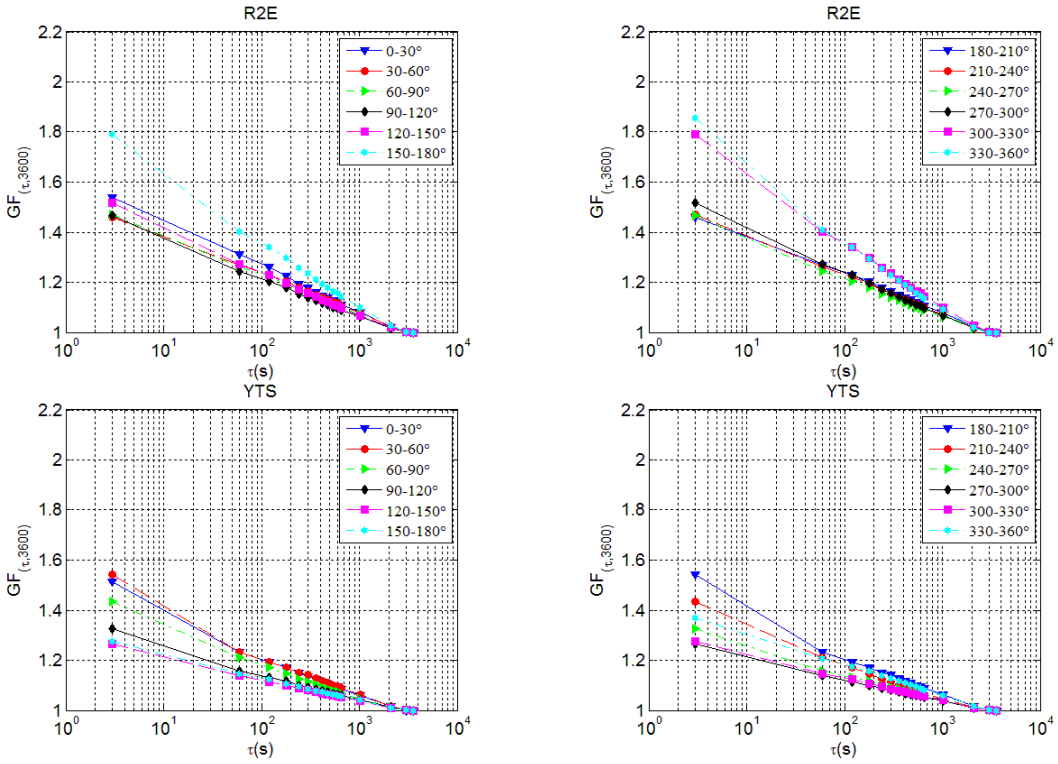

Fig. 10 Gust factor curves of surface windat 4 stations

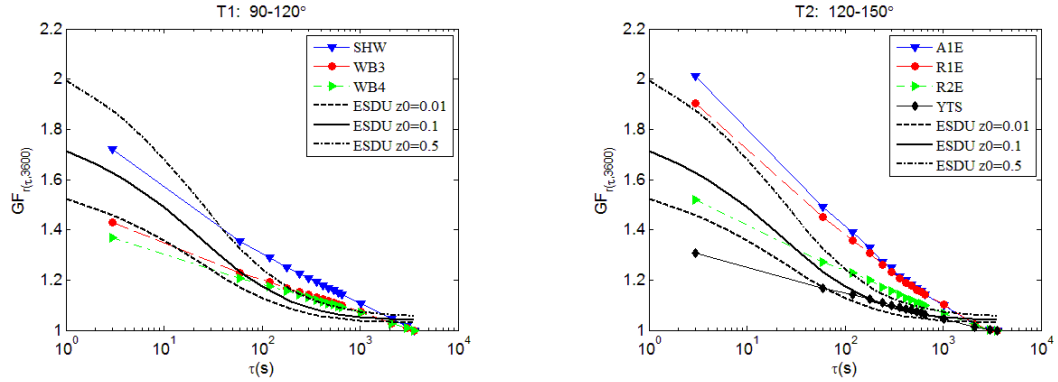

Fig. 11Variations of gust factors along T1 and T2

The azimuthal exposures at WB3, WB4, and R2E are quite smooth, with the corresponding roughness value z_0 being around or less than 0.01 m, while those at SHW, R1E, and A1E turn to be distinctly large (SHW:≈ 0.2 m, R1E:≈ 0.5 m, A1E:>0.5 m). The large gradient of gust factor values along T1 and T2 may be explained by the fast dissipation of vortex and reversed flows during their downward transmission. Along T1, the similar $GF_{(\tau,T_0)}$ values at WB3 and WB4

reflect that the influence of the upwind topography became considerably weak around WB3 which is located about 10 times the hill height away from the hill crest.

6. Canyon effect

As shown in Fig. 1, the PKA station in transect T3is located just at the saddle point between two mountain peaks. Thus, the stations in T3, especially the PKA station, are selected to investigate the canyon effect on the characteristics of surface winds. The CCH station is considered as a reference station to provide the reference information.

Wind rose plots of the 6 years' 1min mean horizontal wind records at these four stations are shown in Fig. 12. As can be seen, almost all the wind directions at PKA were constrained within two linearly distributed azimuth sections which are centered around 150° and 330°, respectively. From Fig. 1, these two sections coincide with the canyon opening directions. The annual mean wind speed is found to be 5.94 m/s based on the minute-to-minute updated records, which is larger than those at most of other stations (R1E: 4.39 m/s, R2E: 4.64 m/s, CCH: 4.86 m/s, WGL: 6.24 m/s). Thus, the canyon effect plays a dominated role on the local wind climate around PKA. The records at R1C and R2C were also influenced by the canyon effect. A prevailing wind direction around 150° can also be observed, as marked by the red ellipses in Fig. 12. But this was more evident at R1Cwhich is located nearer the saddle point. At R2C, it turned to be quite weak.

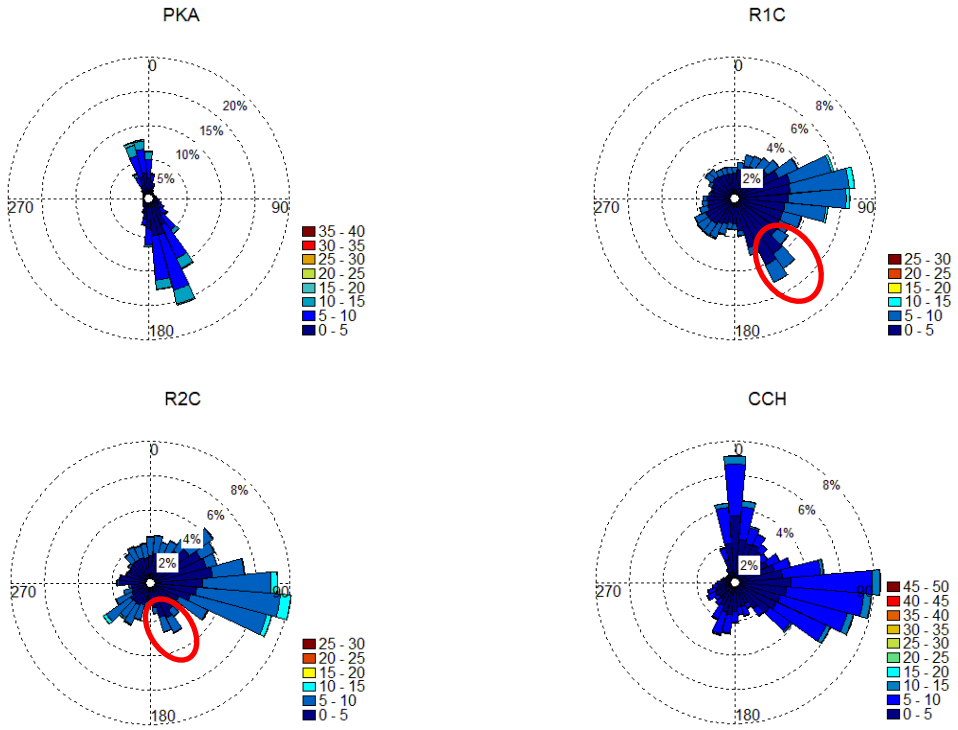

Fig. 12 Wind rose plots based on 6 years' minute-to-minute updated records

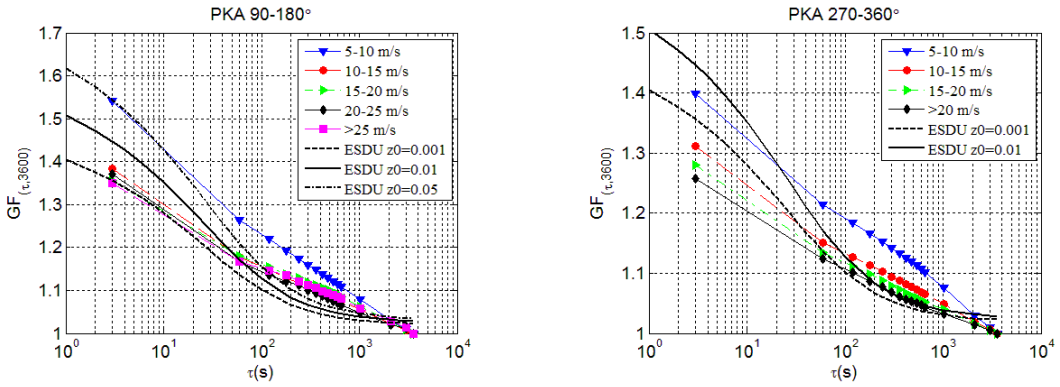

Fig. 13 Gust factor curves of horizontal wind component at PKA

Fig. 13 shows the gust factor curves by groups of mean wind speed at PKA, based on the qualified 1hlength segments selected from the minute-to-minute updated records. Predictions via the ESDU model (ESDU 1983) at 15 m height above open terrains with varied roughness lengths are also depicted. Under weak wind conditions, $GF_{(3,3600)}$ values at these two sections were 1.54 and 1.40, corresponding to 0.05 m and 0.004 m of the estimated roughness lengths. For stronger winds, $GF_{(3,3600)}$ values turned to be smaller, with the corresponding roughness length around or smaller than 0.001 m.

In consideration of more stable wind directions, relatively less turbulent and stronger wind speed at PKA, this site can be regarded as a desirable place of wind farm.

7. Conclusions

This study investigated the topographic effects on the wind characteristics over hilly terrain based on the field measurements collected from a number of meteorological stations in Hong Kong. The main conclusions and findings of this study are summarized as follows:

- Wind characteristics of both mean and turbulent components at the foot of a 3D hill were influenced remarkably in either case of wind blowing from the hilltop to hill-foot (section θ2) or from hill-foot to hilltop (section θ6).
- Profiles of mean horizontal wind speed deviated from the log-law predictions markedly at the upper heights: speeds in section θ2 accompanied with downward movement of flows were more accelerated along altitude, while those in section θ6 with upward flows tended to level off. This feature became more evident when wind speed got larger.
- The log-linear law was adopted to model the mean wind speed profiles. Vertical profiles of both mean wind and turbulent wind were formulated as functions of height and speed.
- Profiles of σ_w/σ_uwere found to differ with the ESDU model predictions remarkably. An empirical model was presented as a function of the half-height length.
- Separations and reversed flows were observed at SHW on the leeward sides of nearby hills.
- The results from two groups of linearly located stations demonstrated that wind turbulence represented by the gust factor values could be affected by nearby hills/mountains markedly. The

nearer to the upwind topographic obstacles, the more evident this effect became. But, such topographic effects turned to be weakened rapidly with the distance being away from the hill crest due to the rapid dissipation of the formed vortices.

- Canyon effect was observed. For the PKA station located at the saddle point of two mountain peaks, the local wind climate was dominated by this effect. There were only two prevailing wind directions which were parallel to the canyon opening orientations. The stable wind direction, less turbulent and stronger wind speed at PKA makes it a suitable place for establishing wind turbines for power generation.

Acknowledgements

The authors would like to express their gratitude to Hong Kong Observatory for the provision of the wind data records and the permission of using the data for this study. The work described in this paper was fully supported by a grant from the Research Grants Council of Hong Kong Special Administrative Region, China (Project No: City U 118213) and a grant from National Natural Science Foundation of China (Project No. 51278439) and a grant from the Research Committee of City University of Hong Kong (Project No: 7002748).

References

Apsley, D.D. and Castro, I.P. (1997), "Flow and dispersion over hills: comparison between numerical predictions and experimental data", *J. Wind Eng. Ind. Aerod.*, **67-68**, 375-386.

Architectural Institute of Japan (2004), AIJ Recommendation for Loads on Building, Japan.

ASCE 7 (2005), *Wind loads*, American Society of Civil Engineers ASCE7-05 Standard.

Baker, C.J. (1984), "Determination of topographical exposure factors in complicated hilly terrain", *J. Wind Eng.Ind. Aerod.*, **17**(2), 239-249.

Baker, C.J., Wood, C.J. and Gawthorpe R.G. (1985), "Strong wind in complicated hilly terrain-field measurements and wind-tunnel study", *J. Wind Eng.Ind. Aerod.*, **18**(1), 1-26.

Beljaars, A.C.M., Walmsley, J.L. and Taylor, P.A. (1987), "A mixed spectral finite-difference model for neutrally stratified boundary-layer flow over roughness changes and topography", *Bound.- Lay. Meteor.*, **38**(3), 273-303.

Bowen, A.J. and Clucas, H. (1992), "The measurement and interpretation of peak-gust wind speeds over an isolated hill", *J. Wind Eng.Ind. Aerod.*, **41-44**, 381-392.

Cao, S.Y. and Tamura, T. (2006), "Experimental study on roughness effects on turbulent boundary layer flow over a two-dimensional steep hill", *J. Wind Eng. Ind. Aerod.*, **94**(1), 1-19.

Cao, S.Y., Wang, T., Ge, Y.J. and Tamura, Y. (2012), "Numerical study on turbulent boundary layers over two-dimensional hills-effects of surface roughness and slope", *J. Wind Eng. Ind. Aerod.*, **104-106**, 342-349.

Chan, P.W. (2008), "Measurement of turbulence intensity profile by a mini-sodar", *Meteorol. Appl.*, **15**(2), 249-258.

Chan, P.W. (2014), "Observation and numerical simulation of vortex/wave shedding for terrain-distributed airflow at the Hong Kong International Airport during Typhoon Nesat in 2011", *Meteorol. Appl.*, **21**, 512-520.

Cochran, L. and Derickson, R. (2011), "A physical modeler's view of computational wind engineering", *J. Wind Eng. Ind. Aerod.*, **99**(4), 139-153.

Coppin, P.A., Bradley, E.F. and Finnigan, J.J. (1994), "Measurements of flow over an elongated ridge and its

thermal stability dependence: the mean field", *Bound.-Lay. Meteor.*, **69**(1-2), 173-199.
Derickson, R.G. and Peterka, J.A. (2004), "Development of a powerful hybrid tool for evaluating wind power in complex terrain: atmospheric numerical models and wind tunnels", *Proceedings of the 23rdASME Wind Energy Symposium*, **15**, Reno, Nevada, USA.
ESDU (1985), Characteristics of atmospheric turbulence near the ground. Part 2: single point data for strong winds (neutral atmosphere). Item No. 85020, ESDU International, London, UK.
ESDU (1983), Strong wind in the atmospheric boundary layer, Part 2: Discrete gust speeds. Item No. 83045, ESDU International, London, UK.
Garratt, J.R. (1992), The Atmospheric Boundary Layer, Cambridge atmospheric and space science series, Cambridge University Press, New York, USA.
GB50009-2012 (2012), China Academy of Building Research, National load codes for the design of building structures, China Architectural & Building Press, Beijing, China.
Griffiths, A.D. and Middleton, J.H. (2010), "Simulations of separated flow over two dimensional hills", *J. Wind Eng.Ind. Aerod.*, **98**(3), 155-160.
He, Y.C., Chan, W.P. and Li, Q.S. (2013), "Wind characteristics under different terrain conditions", *J. Wind Eng. Ind. Aerod.*, **120**, 51-69.
Hunt, J.C.R., Abell, C.J., Peterka, J.A. and Woo, H. (1978), "Kinematical studies of the flows around free or surface-mounted obstacles; applying topology to flow visualization", *J. Fluid Mech.*, **86**(1), 179-200.
Hunt, J.C.R., Leibovich, S. and Richards, K.J. (1988), "Turbulent shear flows over low hills", *Q. J. Roy. Meteor. Soc.*, **114**(484), 1435-1470.
Hunt, J.C.R. and Richards, K.J. (1984), "Stratified airflow over one or two hills", *Bound.- Lay. Meteor.*, **30**, 223-259.
Jackson, P.S. and Hunt, J.C.R. (1975), "Turbulent wind flow over a low hill", *Q. J. Roy. Meteor. Soc.*, **101**(430), 929-955.
Keith, W.A. and Dale, E.H. (2004), "Observations of boundary-layer wind-tunnel flow over isolated ridges of varying steepness and roughness", *Bound.- Lay. Meteor.*, **112**(3), 525-556.
Kustas, W.P. and Brutsaert, W. (1986), "Wind profile constants in a neutral atmospheric boundary layer over complex terrain", *Bound.-Lay. Meteor.*, **34**(1-2), 35-54.
Lemelin, D.R., Surry, D. and Davenport, A.G. (1988), "Simple approximations for wind speed-up over hills", *J. Wind Eng.Ind. Aerod.*, **28**(1-3), 117-127.
Mason, P.J. and Sykes, R.I. (1979), "Flow over an isolated hill of moderate slope", *Q. J. Roy. Meteor. Soc.*, **105**(444), 383-395.
Mason, P. J. and King, J. C. (1985), "Measurements and predictions of flow and turbulence over an isolated hill of moderate slope", *Quart. J. Roy. Meteor. Soc.*, **111**(468), 617-640.
Masters, F.J., Vickery, P.J., Bacon, P. and Rappaport, E.N. (2010), "Toward objective, standardized intensity estimates from surface wind speed observations", *B. Am. Meteorol. Soc.*, **91**(12), 1665-1681.
Mengelkamp, H.T. (1999), "Wind climate simulation over complex terrain and wind turbine energy output estimation", *Theor. Appl. Climatol.*, **63**(3-4), 129-139.
Mickle, R.E., Cook, N.J., Hoff, A.M., Jensen, N.O., Salmon, J.R., Taylor, P.A., Tetzlaff, G. and Tunissen, H.W. (1988), "The Askervein Hill Project: vertical profiles of wind and turbulence", *Bound.- Lay. Meteor.*, **43**(1-2), 143-169.
Ngo, T. and Letchford, C. (2008), "A comparison of topographic effects on gust wind speed", *J. Wind Eng. Ind. Aerod.*, **96**(12), 2273-2293.
Powell, M.D., Vickery, P.J. and Reinhold, T.A. (2003), "Reduced drag coefficient for high wind speeds in tropical cyclones", *Nature*, **422**, 279-283.
Salmon, J.R., Bowen, A.J., Hoff, A.M., Johnson, R., Mickle, R.E., Taylor, P.A., Tetzlaff, G. and Walmsley, J.L. (1988), "The Askervein Hill Project: mean wind variations at fixed heights above ground", *Bound.- Lay. Meteor.*, **43**(3), 247-271.
Stearns, C.R. (1970), "Determining surface roughness and displacement height", *Bound.- Lay. Meteor.*, **1**(1), 102-111.

Tamura, T., Cao, S.Y. and Okuno, A. (2007a), "LES study of turbulent boundary layer over a smooth and a rough 2D hill model", *Flow Turbul. Combust.*, **79**(4), 405-432.
Tamura, T., Okuno, A. and Sugio, Y. (2007b), "LES analysis of turbulent boundary layer over 3D steep hill covered with vegetation", *J. Wind Eng.Ind. Aerod.*, **95**(9-11), 1463-1475.
Tamura, Y., Iwatani, Y., Hibi, K., Suda, K., Nakamura, O., Maruyama, T. and Ishibashi, R. (2007), "Profiles of mean wind speeds and vertical turbulence intensities measured at seashore and two inland sites using Doppler SODAR", *J. Wind Eng.Ind. Aerod.*, **95**(6), 411-427.
Takahashi, T., Ohtsu, T., Yassin, M.F. and Kato, S. (2002), "Turbulence characteristics of wind over a hill with a rough surface", *J. Wind Eng.Ind. Aerod.*, **90**(12-15), 1697-1706.
Taylor, P.A., Mason, P.J. and Bradley, E.F. (1987), "Boundary-layer flow over low hills", *Bound.- Lay. Meteor.*, **39**(1-2), 107-132.
Taylor, P.A. and Teunissen, H.W. (1987), "The Askervein Hill Project: overview and background data", *Bound.- Lay. Meteor.*, **39**(1-2), 15-39.
Taylor, P.A. (1998), "Turbulent boundary-layer flow over low and moderate slope hills", *J. Wind Eng. Ind. Aerod.*, **74-76**, 25-47.
Walmsley, J.L., Salmon, J.R. and Taylor, P.A. (1982), "On the application of a model of boundary-layer flow over low hills to real terrain", *Bound.- Lay. Meteor.*, **23**(1), 17-46.
Walmsley, L. and Taylor P.A. (1996), "Boundary-layer flow over topography: impacts of the Askervein study", *Bound.-Lay. Meteor.*, **78**, 291-320.
Wiggs, G.F.S., Livingstone, I, Thomas, D.S.G. and Bullard, J.E. (1996), "Airflow and roughness characteristics over partially vegetated linear dunes in the southwest Kalahari Desert", *Earth Surf. Proc. Land.*, **21**, 19-34.
Wood, N. (1995), "The onset of separation in neutral, turbulent flow over hills", *Bound.- Lay. Meteor.*, **76**(1-2), 137-164.
Wood, N. (2000), "Wind flow over complex terrain: a historical perspective and the prospect for large-eddy modeling", *Bound.- Lay. Meteor.*, **96**(1-2), 11-32.
Xu, D., Ayotte, K.W. and Taylor, P.A. (1994), "Development of the NLMSFD model of turbulent boundary-layer flow over topography", *Bound.- Lay. Meteor.*, **70**, 341-367.

CC